

Repurposing Video Diffusion Transformers for Robust Point Tracking

Soowon Son¹ Honggyu An¹ Chaehyun Kim¹ Hyunah Ko¹ Jisu Nam¹
 Dahyun Chung¹ Siyoon Jin¹ Jung Yi¹ Jaewon Min¹ Junhwa Hur^{2†} Seungryong Kim^{1†}

¹KAIST AI ²Google DeepMind

<https://cvlab-kaist.github.io/DiTracker>

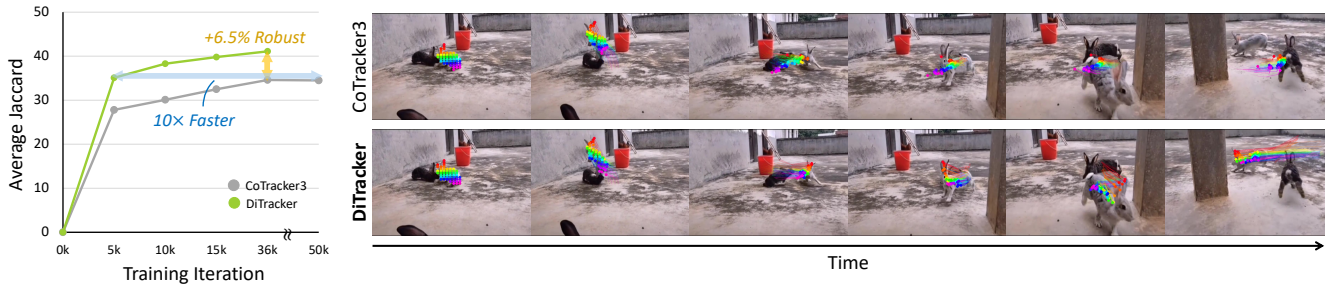


Figure 1. **Enhanced robustness and training efficiency of our DiT-based point tracking framework.** DiTracker leverages pre-trained video Diffusion Transformer (DiT) features to outperform state-of-the-art methods such as CoTracker3 [26] in challenging real-world scenarios involving complex motion and frequent occlusions, while achieving comparable final performance with **10× faster convergence**, substantially reducing training cost. These results demonstrate that pre-trained video DiT features constitute an effective and efficient foundation for robust point tracking.

Abstract

Point tracking aims to localize corresponding points across video frames, serving as a fundamental task for 4D reconstruction, robotics, and video editing. Existing methods commonly rely on shallow convolutional backbones such as ResNet that process frames independently, lacking temporal coherence and producing unreliable matching costs under challenging conditions. Through systematic analysis, we find that video Diffusion Transformers (DiTs), pre-trained on large-scale real-world videos with spatio-temporal attention, inherently exhibit strong point tracking capability and robustly handle dynamic motions and frequent occlusions. We propose **DiTracker**, which adapts video DiTs through: (1) query-key attention matching, (2) lightweight LoRA tuning, and (3) cost fusion with a ResNet backbone. Despite training with 8× smaller batch size, DiTracker achieves state-of-the-art performance on challenging ITTO benchmark and matches or outperforms state-of-the-art models on TAP-Vid benchmarks. Our work validates video DiT features as an effective and efficient foundation for point tracking.

1. Introduction

Point tracking [7, 8, 11, 12, 19, 26, 29, 58, 64] aims to localize corresponding points across video frames, serving as a foundation for a wide range of downstream tasks, e.g., 4D reconstruction [57], robotics [54], and video editing [15]. Existing methods commonly follow a standard design [7, 26]: a feature backbone extracts per-frame features, local matching costs are computed, and a tracking head refines trajectories given these costs. Consequently, performance relies heavily on the quality of matching costs provided by the feature backbone.

Current methods, however, suffer from fundamental limitations in their feature backbones. They predominantly rely on shallow convolutional architectures (e.g. ResNet [20]) that process frames independently, resulting in lacking temporal coherence across the video sequence. This temporal inconsistency produces unreliable matching costs, particularly large displacements between frames. The problem is further compounded by training primarily on synthetic datasets [17], which lack the complexity of real-world scenarios. Together, these issues limit robustness under challenges such as dynamic motions and occlusions.

On the other hand, video Diffusion Transformers (DiTs) [36, 55, 61] have demonstrated remarkable capabilities in generating temporally consistent videos where iden-

[†]Co-corresponding.

tical physical points remain coherent across frames. This property has motivated their adaptation as feature backbones for geometric tasks [14, 28, 41, 43, 52, 59, 62]. Video DiTs offer two key advantages for feature backbones: (1) *spatio-temporal attention* that enables direct feature interaction and internal point correspondence [44], and (2) *large-scale training on real-world videos* that captures generalizable motion priors. These characteristics suggest ***pre-trained video DiTs could serve as robust feature backbones for point tracking*** through more reliable temporal correspondence.

To investigate their potential, we systematically analyze pre-trained video DiT features [36, 55, 61] for robustness in real-world scenarios. Our analysis reveals that video DiT features produce significantly more accurate initial matches than ResNet features [26] explicitly trained on point tracking data. We also assess performance under challenging real-world conditions including motion blur, large displacements, and frequent occlusions. Across all conditions, video DiT features consistently outperform supervised ResNet features in challenging real-world conditions. These findings demonstrate that large-scale video pre-training with spatio-temporal attention provides critical advantages for real-world generalization, even surpassing task-specific supervision.

Based on these analyses, we propose **DiTracker**, which adapts video DiT features for point tracking through three key designs. First, we compute matching costs using query-key attention with softmax normalization, mirroring DiT’s internal attention mechanism [44] to preserve its inherent matching capability. Second, we employ lightweight LoRA tuning [24] to efficiently adapt the DiT backbone without disrupting its learned temporal correspondence. Third, we introduce a cost fusion strategy that combines DiT and ResNet features to leverage their complementary strengths: DiT provides robust global matching under challenging conditions such as large displacements, frequent occlusions, while ResNet captures fine-grained local details. This framework enables effective adaptation of video DiT features for point tracking.

We evaluate DiTracker on TAP-Vid-DAVIS [11], TAP-Vid-Kinetics [11], and the challenging real-world benchmark ITTO [9]. While TAP-Vid benchmarks primarily consist of static points and low frequent occlusions, ITTO features challenging scenarios with tracks categorized by motion dynamics and occlusion frequency. We additionally evaluate on TAP-Vid-DAVIS with ImageNet-C [21] visual corruptions to assess robustness. Despite training with 8× smaller batch size than state-of-the-art methods, DiTracker achieves substantial improvements on ITTO and matches or exceeds state-of-the-art on TAP-Vid benchmarks. On corruption benchmarks, DiTracker consistently matches or exceeds state-of-the-art performance. These results demon-

strate that video DiT features provide an effective and efficient backbone for point tracking.

In summary, our contributions are as follows:

- We systematically analyze pre-trained video DiT features for point tracking, demonstrating superior robustness compared to supervised ResNet backbones.
- We propose **DiTracker**, which effectively adapts video DiT features for point tracking through query-key matching, lightweight LoRA tuning, and cost fusion with ResNet for complementary strengths.
- We achieve state-of-the-art performance on the challenging ITTO benchmark with 8× smaller batch size, while matching or exceeding state-of-the-art on TAP-Vid benchmarks and corruption robustness tests.

2. Related Work

Point tracking. Building on the classic Particle Video [49], PIPs [18] introduced a learning-based point tracking approach that iteratively refines initial matches derived from local matching costs. TAPIR [12] advanced this paradigm by first establishing global correspondences via TAP-Net [11] and then refining them using a PIPs-style iterative module. Subsequent works have expanded this framework through architectural redesign [33, 34, 47], multi-point interaction [26, 27], enhanced receptive fields [7], 3D extensions [8, 58], optical-flow integration [6, 32], and test-time optimization [53, 56]. Despite these advancements, most models are trained on synthetic datasets such as Kubric [17], limiting their robustness under real-world conditions due to domain mismatch. To mitigate this gap, recent works such as BootsTAP [13] and CoTracker3 [26] incorporate real-world videos via semi-supervised learning, while others [4, 25, 30] attempt to generate real-world tracking datasets. However, these efforts remain constrained by limited domain diversity or by the performance ceilings of the trackers used for annotation.

Feature backbones for point tracking. While recent progress has focused on sophisticated refinement modules [7, 11, 12, 27], most methods still depend on fixed backbones such as ResNet [20] or TSM-ResNet [37], leaving the potential of stronger feature extractors underexplored. Addressing this, several works have investigated DINOv2 [45] as a backbone, demonstrating substantial gains for point tracking [3, 29, 53]. More broadly, Aydemir et al. [2] showed that representations from diverse vision foundation models can further improve tracking quality, with Stable Diffusion [48] features even surpassing DINOv2. In the same direction, DiffTrack [44] revealed that video diffusion transformers (DiTs), even without explicit supervision for the tracking task, possess layers highly aligned with temporal correspondence and outperform conventional backbones in zero-shot settings. Building on

these insights, our work exploits video DiTs as powerful feature backbones and integrates their representations seamlessly into existing point tracking frameworks.

Diffusion models for geometric tasks. Beyond generation, large-scale pre-training endows diffusion models with rich representations [22, 48] applicable to geometric tasks such as visual correspondence [14, 41, 43, 52, 62], segmentation [59], and depth estimation [28]. Pioneering approaches such as DIFT [52] and SD-DINO [62] demonstrated that diffusion models inherently encode semantic and geometry aware features, achieving competitive zero-shot correspondence performance. Subsequent studies have further strengthened these capabilities through architectural modifications [39, 40, 60, 63], distillation [51], and prompt tuning [35]. This research suggests diffusion models can generalize to perception tasks with minimal supervision with synthetic dataset [28], reducing the sim-to-real gap that limits conventional point tracking backbones. We extend this insight by repurposing video diffusion features to achieve robust tracking using only sparse, high-quality synthetic data.

3. Preliminary

Video diffusion transformers. Video DiTs consist of a VAE and a denoising transformer. Given a video sequence $X \in \mathbb{R}^{F \times H \times W \times 3}$, the VAE encodes X into latent representations $\mathbf{z}_{\text{video}} \in \mathbb{R}^{f \times h \times w \times d_{\text{video}}}$, where $(F, H, W, 3)$ denote the number of frames, height, width, and RGB channels, and $(f, h, w, d_{\text{video}})$ denote the corresponding latent dimensions. During the diffusion process, Gaussian noise $\epsilon \sim \mathcal{N}(0, I)$ is added to $\mathbf{z}_{\text{video}}$, and the denoising transformer v_{θ} learns to predict the velocity field that maps noisy latents back to clean ones via flow matching [38].

Full 3D attention in video DiTs. At each transformer layer l and attention head m in the denoising transformer network, the i -th frame latent is projected into query and key matrices:

$$Q_i^{l,m}, K_i^{l,m} \in \mathbb{R}^{h \times w \times d_{\text{head}}}, \quad (1)$$

where d_{head} is the channel dimension per head. The attention mechanism computes a matching cost $\mathcal{C}_{i,j}^{l,m} \in \mathbb{R}^{h \times w \times h \times w}$ between the i -th and j -th frame latents as

$$\mathcal{C}_{i,j}^{l,m} = \text{Softmax} \left(\frac{Q_i^{l,m} (K_j^{l,m})^\top}{\sqrt{d_{\text{head}}}} \right), \quad (2)$$

where $\mathcal{C}_{i,j}^{l,m}$ captures the interactions between the query of the i -th frame and key of the j -th frame [42, 44].

4. Analysis

We argue that video DiT features inherently exhibit strong generalizability in challenging real-world settings, benefiting from large-scale real-video pretraining and a full 3D at-

Table 1. **Zero-shot point tracking performance comparison on TAP-Vid-DAVIS benchmark [11].** Compared to the supervised ResNet from CoTracker3 [26] and other vision foundation models [1, 45, 50], video DiTs [31, 55, 61] show superior performance. Best, second best and third best are highlighted.

Method	$< \delta^0$	$< \delta^1$	$< \delta^2$	$< \delta^3$	$< \delta^4$	δ_{avg}^x
ResNet (CoTracker3 [26])	10.5	34.0	49.7	57.7	66.6	43.7
V-JEPA2 [1]	2.8	10.5	30.5	55.4	69.9	33.8
DINOv2-B/14 [45]	2.8	10.9	35.6	67.2	83.5	40.0
DINOv3-B/16 [50]	3.0	11.8	37.7	68.2	84.7	41.1
HunyuanVideo [31]	4.4	18.2	44.8	70.1	82.8	44.1
CogVideoX-2B [61]	4.8	19.4	49.2	73.6	86.3	46.3
CogVideoX-5B [61]	5.2	20.5	50.7	73.9	84.3	46.9
WAN-14B [55]	12.4	31.9	56.7	72.1	82.7	51.2

tention architecture. We investigate several video DiT models, including HunyuanVideo [31], CogVideoX-2B [61], CogVideoX-5B [61], and WAN-14B [55], and compare them with the supervised ResNet [20] feature backbone from CoTracker3 [26], which is explicitly trained for point tracking. We also evaluate other vision foundation models, V-JEPA2 [1], DINOv2-B/14 [45], and DINOv3-B/16 [50], with additional details provided in Appendix A.

4.1. Temporal Correspondence in Video DiTs

Following Nam et al. [44], we extract point trajectory using pre-trained video DiTs features. To avoid VAE temporal compression, we encode each frame $X_i \in \mathbb{R}^{H \times W \times 3}$ independently to obtain per-frame latents $\mathbf{z}_i \in \mathbb{R}^{h \times w \times d_{\text{video}}}$. We then extract query-key features at a specific layer l and attention head m at the final denoising timestep as in Eq. (1). Here, we select the optimal layer l and head m by analyzing zero-shot point tracking performance across all layers and heads (Appendix B.1).

We construct the matching cost $\mathcal{C}_{1,j}^{l,m}$ as in Eq. (2) and find corresponding points P_j in the j -th frame for starting point P_1 in the first frame via argmax operation (Argmax):

$$P_j = \text{Argmax}_{p \in \Omega} \mathcal{C}_{1,j}^{l,m}(P_1, p), \quad (3)$$

where Ω is the spatial domain. Final point trajectories are obtained by concatenating the starting point with estimated matches, then upscaling to original coordinates through linear interpolation (Interp):

$$\mathcal{T}_{1:F} = \text{Interp}(\text{Concat}(P_1, P_2, \dots, P_F)). \quad (4)$$

We then measure accuracy with percentage of correctly tracked points across multiple distance thresholds (1, 2, 4, 8, and 16), averaged to δ_{avg}^x .

4.2. Robustness in Real-World Scenarios

Table 1 compares point tracking performance across different feature backbones and the supervised ResNet from CoTracker3 in a zero-shot fashion on TAP-Vid-DAVIS [11].

Table 2. **Zero-shot robustness analysis across challenging scenarios TAP-Vid-DAVIS [11] and ITTO-MOSE [9] benchmarks**, including the supervised ResNet from CoTracker3 [26], video DiTs [31, 55, 61], and other vision foundation models [1, 45, 50]. **Motion Blur**: Performance under ImageNet-C motion blur [21] at severity levels 1-5 on TAP-Vid-DAVIS. **Motion Dynamics**: Accuracy across displacement categories on ITTO-MOSE—static [0%, 0.5%), normal [0.5%, 1.5%), dynamic [1.5%, 5%). **Reappearance Frequency**: Performance across occlusion frequency categories on ITTO-MOSE—low [0, 1), medium [1, 3), high [3, 1000). In this analysis, video DiTs consistently demonstrate superior robustness compared to the ResNet in supervised CoTracker3 and other foundation models across all scenarios. All metrics reported as δ_{avg}^x . Best, second best and third best are highlighted.

Method	Motion Blur					Motion Dynamics			Reappearance Frequency		
	1	2	3	4	5	[0%,0.5%)	[0.5%,1.5%)	[1.5%,5%)	[0,1)	[1,3)	[3,100)
ResNet (CoTracker3 [26])	42.4	40.0	36.2	31.0	27.9	24.7	16.7	9.7	22.7	17.1	10.6
V-JEPA2 [1]	29.0	27.3	24.3	20.3	19.0	21.8	23.2	17.4	24.4	20.9	17.0
DINOv2-B/14 [45]	39.0	37.6	34.7	32.4	29.9	24.3	23.5	19.3	23.9	23.6	19.9
DINOv3-B/16 [50]	40.0	38.5	36.5	34.0	31.8	30.1	24.4	20.8	29.1	25.8	20.1
HunyuanVideo [36]	41.7	40.6	38.9	36.4	34.5	42.7	30.7	16.9	40.6	28.7	19.4
CogVideoX-2B [61]	45.0	43.6	41.6	39.0	36.7	45.4	33.7	19.2	43.1	31.7	21.5
CogVideoX-5B [61]	45.5	44.2	42.2	39.5	37.7	44.9	37.4	22.2	44.5	34.1	23.9
WAN-14B [55]	50.7	49.6	47.6	44.6	42.5	46.3	35.3	21.2	43.4	34.3	22.9

Video diffusion models consistently yield superior initial matching quality, with WAN-14B and CogVideoX-2B each achieving 51.2% and 46.3% at δ_{avg}^x compared to 43.7% for the supervised ResNet baseline, despite having no tracking-specific training.

We further assess robustness under challenging conditions by comparing video DiT features and the supervised ResNet from CoTracker3 across three critical scenarios: (1) motion blur, (2) dynamic motions, and (3) frequent occlusions. Table 2 presents comprehensive zero-shot evaluation results.

Motion blur. We apply ImageNet-C motion blur at severity levels 1-5 [21] to TAP-Vid-DAVIS [11]. ResNet degrades significantly by 14.5%p when motion blur severity increases from 1 to 5, while video DiTs maintain stability with only 8.2%p (WAN-14B) and 7.8%p (CogVideoX-5B) degradation. At maximum severity, WAN-14B outperforms ResNet by 14.6%p.

Motion dynamics. We analyze ITTO-MOSE [9] tracks categorized by normalized frame-to-frame displacement. The Motion Dynamics results in Table 2 show that video DiTs consistently outperform ResNet across all motion categories. On dynamic [1.5%, 5%) tracks requiring large displacement handling, CogVideoX-5B achieves 22.2%, substantially exceeding ResNet’s 9.7%.

Reappearance after occlusion. We categorize ITTO-MOSE tracks by reappearance frequency (occlusion-to-visible transitions). The Reappearance Frequency results in Table 2 show that video DiTs substantially outperform ResNet at re-identification. On high-reappearance [3, 1000) tracks, CogVideoX-5B (23.9%) and WAN-14B (22.9%) substantially outperform ResNet (10.6%) by 12.3–13.3%p.

4.3. Key Findings

In results, video DiTs such as HunyuanVideo, CogVideoX-2B/5B, WAN-14B consistently demonstrate superior matching accuracy across all scenarios, substantially outperforming the supervised ResNet. Image-based models like DINOv2-B/14 [45] and DINOv3-B/16 [50] show reasonable performance but exhibit limitations from processing frames independently. V-JEPA2 consistently underperforms across all metrics despite video training.

Our analysis reveals two critical insights. First, video DiT features trained solely with generation objectives on unlabeled videos substantially outperform ResNet features explicitly supervised on point tracking data, demonstrating that large-scale real-world video pretraining produces more generalizable matching costs than supervised training on synthetic datasets suffering from domain gap. Despite this overall superiority, we find that ResNet performs better at fine-grained threshold ($< \delta^0, < \delta^1$ in Table 1) due to its finer spatial resolution. Consequently, combining video DiT and ResNet costs further improves performance by leveraging their complementary strengths. Second, video DiT’s full 3D attention (or spatio-temporal attention) jointly processes spatiotemporal information across frames, enabling temporally consistent features that naturally handle large displacements and maintain point identity through occlusions. In contrast, frame-independent feature backbones process each frame separately, lacking temporal context for robust tracking. The consistent superiority of all video DiTs validates that large-scale pretraining with full 3D attention provides fundamentally stronger motion priors for challenging correspondence tasks.

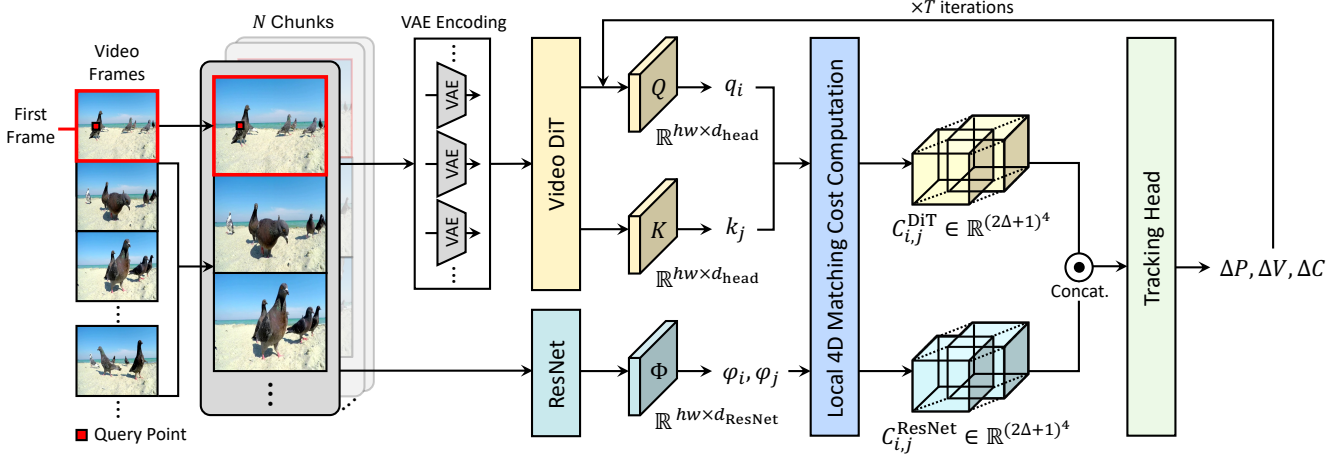


Figure 2. **Overall Architecture of DiTracker.** For long video sequences, input frames are divided into N chunks with the global first frame prepended. Individual video frames are then encoded via VAE. These encoded latents are processed by a video DiT to extract query feature q_i and key feature k_j , which are then used to compute a hierarchical local 4D matching cost $C_{i,j}^{\text{DiT}}$. The video DiT local cost is subsequently fused with the ResNet local cost $C_{i,j}^{\text{ResNet}}$. Finally, a tracking head refines the trajectories over T iterations, updating displacement (ΔP), visibility (ΔV), and confidence (ΔC).

5. DiTracker

Based on the above observations, we introduce **DiTracker**, a simple yet effective method for robust point tracking using video DiT features. Given a video sequence $\mathbf{X} \in \mathbb{R}^{F \times H \times W \times 3}$ with F frames of spatial resolution $H \times W$, our point tracker estimates the trajectory of a query point $\mathbf{p} = (\mathbf{x}, \mathbf{y})$ specified in a query frame. The goal is to predict its positions $\{P_i = (x_i, y_i)\}_{i=1}^F$ across all frames along with visibility $\{V_i \in [0, 1]\}_{i=1}^F$ and confidence $\{C_i \in [0, 1]\}_{i=1}^F$.

5.1. Diffusion Feature Extraction

To efficiently process long videos, we divide the video sequence into N chunks and prepend the first frame X_1 as a shared anchor to each chunk, ensuring consistent query-key feature distributions. We apply Low Rank Adaptation (LoRA) [24] to all layers up to and including layer l , and then extract the query-key features $Q_i^{l,m}, K_i^{l,m}$ from the adapted video DiT, as described in Sec. 4.1.

5.2. Local 4D Matching Cost Computation

We construct a hierarchical local cost pyramid with varying receptive fields to capture multi-scale query-key relationships. To build a feature pyramid with S scales, we interpolate features to resolution $\frac{H}{r \times 2^{s-1}} \times \frac{W}{r \times 2^{s-1}}$, where r denotes the model stride and $s \in \{1, \dots, S\}$ is the scale factor. For notational simplicity, we omit layer and head indices:

$$Q_i^s = \text{Interpolate}^s(Q_i), \quad (5)$$

$$K_i^s = \text{Interpolate}^s(K_i), \quad (6)$$

where $Q_i^s, K_i^s \in \mathbb{R}^{\frac{H}{r \times 2^{s-1}} \times \frac{W}{r \times 2^{s-1}} \times d_{\text{head}}}$ are interpolated query and key features at scale s . At each scale s , we ex-

tract local features around points of interest using bilinear sampling. Local query features q_i^s are sampled within a Δ -sized neighborhood centered at the query point $\mathbf{p} = (\mathbf{x}, \mathbf{y})$ in the query frame i :

$$q_i^s = \left[Q_i^s \left(\frac{\mathbf{x}}{r \times 2^{s-1}} + \delta, \frac{\mathbf{y}}{r \times 2^{s-1}} + \delta \right) : \|\delta\|_\infty \leq \Delta \right], \quad (7)$$

and local key features k_j^s are sampled around the estimated point $P_j = (x_j, y_j)$ across all frame indices $j \in \{1, \dots, F\}$:

$$k_j^s = \left[K_j^s \left(\frac{x_j}{r \times 2^{s-1}} + \delta, \frac{y_j}{r \times 2^{s-1}} + \delta \right) : \|\delta\|_\infty \leq \Delta \right], \quad (8)$$

where $\delta \in \mathbb{Z}$ and $q_i^s, k_j^s \in \mathbb{R}^{d_{\text{head}} \times (2\Delta+1)^2}$.

We then construct a *local 4D matching cost* $C_{i,j}^{s, \text{DiT}}$ between local features of the query frame i and target frame j with softmax operation:

$$C_{i,j}^{s, \text{DiT}} = \text{Softmax} \left(\frac{q_i^s (k_j^s)^\top}{\sqrt{d_{\text{head}}}} \right) \in \mathbb{R}^{(2\Delta+1)^4}. \quad (9)$$

5.3. Matching Cost Fusion

As discussed in Sec. 4.3, we fuse matching costs from video DiT and ResNet features to leverage their complementary strengths. Rather than concatenating feature maps along the channel dimension, which disrupts the pre-trained cost distribution from video DiT, we compute matching costs separately from each backbone and fuse them at the cost level.

For ResNet, we follow the same pipeline as DiT. We extract ResNet features $\Phi_i = \text{ResNet}(X_i)$, construct a multi-scale feature pyramid, and sample local features φ_i^s and φ_j^s

around the query point \mathbf{p} in frame i and around the estimated point P_j in frame j , respectively (following Equations 7 and 8). The local matching cost is:

$$\mathcal{C}_{i,j}^{s,\text{ResNet}} = \text{Softmax} \left(\frac{\varphi_i^s(\varphi_j^s)^\top}{\sqrt{d_{\text{ResNet}}}} \right) \in \mathbb{R}^{(2\Delta+1)^4}, \quad (10)$$

where d_{ResNet} is the channel dimension of ResNet features.

We flatten and concatenate the DiT and ResNet matching costs to obtain the fused cost:

$$\mathcal{C}_{i,j}^{s,\text{fused}} = \left[\text{Flatten}(\mathcal{C}_{i,j}^{s,\text{DiT}}), \text{Flatten}(\mathcal{C}_{i,j}^{s,\text{ResNet}}) \right] \in \mathbb{R}^{2(2\Delta+1)^4}. \quad (11)$$

Finally, we project costs from all scales to cost embeddings E_j using an MLP:

$$E_j = \text{MLP}(\mathcal{C}_{i,j}^{1,\text{fused}}, \dots, \mathcal{C}_{i,j}^{S,\text{fused}}) \in \mathbb{R}^{d_E}, \quad (12)$$

where d_E is the channel dimension of cost embeddings.

5.4. Trajectory Estimation

We finally estimate point trajectories using an iterative transformer-based refinement module following [26]. We first initialize trajectories by broadcasting the query point location to all frames with zero visibility and confidence. At each iteration t , we then calculate per-frame displacement embeddings $\eta_{i \rightarrow i+1} = \eta(P_{i+1} - P_i)$ using Fourier Encoding η , then construct input tokens G_i by concatenating displacement embeddings $\eta_{i-1 \rightarrow i}$ and $\eta_{i \rightarrow i+1}$, visibility V_i , confidence C_i , and cost embeddings E_i for every query point \mathbf{p} . A tracking head Ψ with factorized temporal and query-point attention processes these tokens to predict residual updates: $P^{(t+1)} = P^{(t)} + \Delta P^{(t)}$, $V^{(t+1)} = V^{(t)} + \Delta V^{(t)}$, $C^{(t+1)} = C^{(t)} + \Delta C^{(t)}$, where $\Delta P^{(t)}, \Delta V^{(t)}, \Delta C^{(t)} = \Psi(G)$. After each update, we re-sample correlation features at the refined locations. After T iterations, we obtain the final trajectory predictions $\{P_i, V_i, C_i\}_{i=1}^F$.

5.5. Training Loss

Our training objective consists of three complementary loss terms that supervise trajectory estimation, visibility, and confidence prediction across all refinement iterations as $\mathcal{L} = \mathcal{L}_{\text{track}} + \mathcal{L}_{\text{vis}} + \mathcal{L}_{\text{conf}}$.

Trajectory supervision. We supervise coordinate predictions for both visible and occluded points using the Huber loss $\text{Huber}(\cdot)$ with a 6-pixel threshold. To encourage the model to focus on accurately tracking visible points, we apply asymmetric weighting based on occlusion state:

$$\mathcal{L}_{\text{track}} = \sum_{t=1}^T \gamma^{T-t} \left(\frac{\mathbb{1}_{\text{occ}}}{5} + \mathbb{1}_{\text{vis}} \right) \cdot \text{Huber}(P^{(t)}, \hat{P}), \quad (13)$$

where $P^{(t)}$ denotes predicted coordinates at iteration $t \in \{1, \dots, T\}$, \hat{P} is the ground truth, $\mathbb{1}_{\text{occ}}$ and $\mathbb{1}_{\text{vis}}$ are indicator functions for occluded and visible states, and $\gamma = 0.8$ is a temporal discount factor that assigns higher importance to later refinement stages. This weighting scheme assigns 5× lower weight to occluded points, prioritizing accurate tracking of visible points.

Visibility supervision. Visibility predictions are supervised with Binary Cross Entropy (BCE) loss $\text{CE}(\cdot)$ using ground truth visibility annotations:

$$\mathcal{L}_{\text{vis}} = \sum_{t=1}^T \gamma^{T-t} \text{CE}(\sigma(V^{(t)}), \hat{V}), \quad (14)$$

where $V^{(t)}$ and \hat{V} denote predicted and ground truth visibility respectively, and $\sigma(\cdot)$ is the sigmoid function applied to visibility logits $V^{(t)}$.

Confidence supervision. We supervise confidence scores using BCE loss. For each iteration, the ground truth confidence label is defined by whether the current prediction falls within 12 pixels of the ground truth location:

$$\mathcal{L}_{\text{conf}} = \sum_{t=1}^T \gamma^{T-t} \text{CE}(\sigma(C^{(t)}), \mathbb{1}[\|P^{(t)} - \hat{P}\|_2 < 12]), \quad (15)$$

where $\sigma(\cdot)$ is the sigmoid function applied to confidence logits $C^{(t)}$.

6. Experiments

6.1. Implementation Details

We train our model on the Kubric MOVi-F dataset [17] for 36k iterations using 4 NVIDIA RTX A6000 GPUs with a maximum sequence length of 46 frames, batch size of 4, and input resolution of 480×720. This resolution is chosen based on CogVideoX-2B’s strong zero-shot performance. Despite modest hyperparameters due to computational constraints—smaller batch sizes and shorter sequences than prior work—our results demonstrate that video DiT features enable state-of-the-art performance even under limited training conditions. Details for hyperparameters and layer, head selection are in Appendix B.1.

6.2. Evaluation Protocol

We evaluate on three benchmarks: TAP-Vid-DAVIS [11], TAP-Vid-Kinetics [11], and ITTO-MOSE [9]. TAP-Vid-DAVIS consists of 30 videos from the DAVIS 2017 validation set [46], while TAP-Vid-Kinetics comprises 1,144 YouTube videos from the Kinetics-700-2020 validation set [5]. Although widely used, the TAP-Vid benchmark has known limitations for assessing real-world robustness [9]: the majority of points are static, and tracks rarely require re-identification after occlusion.

Table 3. **Quantitative results comparison on ITTO-MOSE [9], TAP-Vid-DAVIS [11] and TAP-Vid-Kinetics [11].** Our method trained solely on Kubric (Kub.) with 36k steps significantly outperforms the other baselines. Crucially, our method also surpasses the large-scale pretrained CoTracker3[†], which is trained on Kub. and an additional 15K real-world videos for 65K steps, on the challenging ITTO-MOSE dataset—despite CoTracker3’s substantial advantages in dataset size, training steps, and batch size. Best, second best and third best are highlighted.

Method	Training Dataset	Steps	Sequence Length	Batch Size	ITTO-MOSE			TAP-Vid-DAVIS			TAP-Vid-Kinetics		
					AJ↑	$\delta_{\text{avg}}^x \uparrow$	OA↑	AJ↑	$\delta_{\text{avg}}^x \uparrow$	OA↑	AJ↑	$\delta_{\text{avg}}^x \uparrow$	OA↑
TAPIR [12]	Kub.	50k	24	4	33.1	46.1	75.9	56.2	70.0	86.5	49.6	64.2	85.0
TAPTRv2 [34]	Kub.	44k	-	32	36.3	47.8	76.9	63.0	76.1	91.1	49.0	64.4	85.2
BootsTAPIR [13]	Kub. + 15M	200k	24	1,536	36.9	51.1	76.4	61.4	73.6	88.7	54.6	68.4	86.5
LocoTrack [7]	Kub.	400k	24-48	8	39.2	52.3	78.2	64.8	77.4	86.2	52.3	66.4	82.1
CoTracker3 [26]	Kub.	50k	60	32	34.0	47.1	71.7	57.8	74.9	80.4	49.3	62.7	78.7
CoTracker3 [†] [26]	Kub. + 15k	65k	60-80	32	42.4	55.8	80.4	64.8	76.8	91.7	54.7	67.8	87.5
DiTracker	Kub.	36k	46	4	43.9	57.9	79.3	62.7	77.5	85.2	54.3	67.4	84.5

To address these limitations, we additionally evaluate on ITTO [9], a benchmark designed specifically for challenging real-world tracking scenarios. ITTO comprises videos from MOSE [10], LVOS [23], and Ego4D [16] video object segmentation datasets, featuring more dynamic content and frequent occlusions. We use the MOSE subset consisting of 44 videos with verified annotations. Beyond overall metrics, we analyze performance across different motion dynamics and reappearance rates to assess robustness under varying challenge levels.

To evaluate robustness to visual artifacts, we apply corruptions from ImageNet-C [21] to TAP-Vid-DAVIS videos following [43]. We test across varying severity levels to examine performance degradation under different corruption intensities.

We adopt Average Jaccard (AJ), averaged tracking accuracy (δ_{avg}^x), and Occlusion Accuracy (OA) as the evaluation metrics established by the TAP-Vid benchmark [11]. More details are in Appendix B.2.

6.3. Main Results

Overall benchmark performance. Table 3 presents comprehensive results on ITTO-MOSE [9], TAP-Vid-DAVIS [11], and TAP-Vid-Kinetics [11]. DiTracker trained solely on Kubric synthetic data achieves state-of-the-art or competitive performance across all benchmarks. On ITTO-MOSE, DiTracker achieves 43.9% AJ and 57.9% δ_{avg}^x exceeding CoTracker3 trained with additional real videos. On TAP-Vid-DAVIS and Kinetics, both DiTracker variants achieve competitive or superior performance compared to CoTracker3. Notably, DiTracker achieves these results using only synthetic data with 8 \times smaller batch size and smallest training iteration, demonstrating superior training efficiency from video DiT features.

Performance across difficulty levels. Table 4 presents detailed ITTO-MOSE results stratified by motion dynamics and reappearance frequency. DiTracker consistently achieves best δ_{avg}^x performance across all categories, with

particularly strong advantages on challenging scenarios. On dynamic tracks requiring large displacement handling, DiTracker achieves 38.5% δ_{avg}^x substantially outperforming all other models. For high-reappearance tracks requiring frequent re-identification after occlusion, DiTracker achieves 37.5% δ_{avg}^x demonstrating robust identity maintenance. Remarkably, these results surpass LocoTrack (400K steps) and BootsTAPIR (15M real videos, 200K steps) while training exclusively on synthetic data with much less training steps, validating the exceptional efficiency of video DiT’s motion priors.

Robustness to visual corruptions. Table 5 evaluates robustness under ImageNet-C [21] corruption on TAP-Vid-DAVIS. DiTracker demonstrates superior robustness across most of corruption categories. DiTracker achieves 65.0% average δ_{avg}^x , outperforming CoTracker3 at 64.7%. This superior corruption handling aligns with recent findings [43] that diffusion features trained on large-scale real-world data are naturally robust to noise and visual degradations, enabling more reliable point tracking under challenging visual conditions that ResNet features trained on clean synthetic data cannot match.

Qualitative comparison. Figure 3 visualizes trajectories of ground truth, CoTracker3, and DiTracker on the ITTO-MOSE benchmark. Under large inter-frame displacements, CoTracker3 frequently loses track or remains stuck at initial query locations. When occluded points reappear, CoTracker3 often fails to re-identify them, resulting in discontinuous trajectories. In contrast, DiTracker maintains robust tracking through large motions and accurately re-identifies points after occlusion. Additional qualitative results on ITTO-MOSE, TAP-Vid-DAVIS, and corruption on TAP-Vid-DAVIS are in Appendix C.

6.4. Ablation Studies

We conduct ablation studies to validate our key design choices. For computational efficiency, all ablations use

Table 4. **Quantitative results on ITTO-MOSE [9] across difficulty levels.** Our method achieves top performance across motion dynamics and reappearance frequency categories, demonstrating particularly strong results on challenging scenarios with large displacements and frequent occlusions. Best, second best and third best are highlighted.

Method	Motion Dynamics												Reappearance Frequency																							
	[0%,0.5%)				[0.5%,1.5%)				[1.5%,5%)				[0,1)				[1,3)				[3,1000)															
	AJ↑	$<\delta_{avg}^x$ ↑	OA↑	AJ↑	$<\delta_{avg}^x$ ↑	OA↑	AJ↑	$<\delta_{avg}^x$ ↑	OA↑	AJ↑	$<\delta_{avg}^x$ ↑	OA↑	AJ↑	$<\delta_{avg}^x$ ↑	OA↑	AJ↑	$<\delta_{avg}^x$ ↑	OA↑	AJ↑	$<\delta_{avg}^x$ ↑	OA↑	AJ↑	$<\delta_{avg}^x$ ↑	OA↑												
TAPIR [12]	48.2	60.9	82.9	36.2	51.9	75.9	17.6	28.9	68.9	49.3	63.1	88.0	33.2	46.9	74.8	17.4	28.9	65.2	51.6	64.6	81.9	41.0	54.0	78.3	20.0	29.3	70.9	58.1	69.1	90.1	33.7	46.9	76.4	17.8	27.8	64.5
BootsTAPIR [13]	52.8	65.1	84.5	42.0	57.0	77.4	19.0	35.1	67.3	56.8	68.3	90.2	36.6	52.0	75.3	17.7	33.5	64.2	54.1	66.8	84.9	42.7	58.3	78.6	24.0	35.5	71.7	55.7	68.6	89.0	39.8	53.4	78.7	22.4	35.2	67.4
LocoTrack [7]	48.7	64.0	79.0	35.1	48.5	67.9	12.8	22.6	63.7	51.1	64.8	82.2	31.2	44.0	70.2	12.4	23.5	59.4	48.7	64.0	79.0	35.1	48.5	67.9	12.8	22.6	63.7	51.1	64.8	82.2	31.2	44.0	70.2	12.4	23.5	59.4
CoTracker3 [26]	56.6	67.5	85.4	44.3	56.8	81.2	23.4	34.4	72.1	59.9	69.1	91.5	40.8	53.5	80.7	20.9	32.8	66.4	56.6	67.5	85.4	44.3	56.8	81.2	23.4	34.4	72.1	59.9	69.1	91.5	40.8	53.5	80.7	20.9	32.8	66.4
DiTracker	56.3	67.8	86.4	46.4	59.4	79.5	24.0	38.5	72.7	61.1	70.4	90.5	41.2	54.9	80.7	21.4	37.5	67.3	56.3	67.8	86.4	46.4	59.4	79.5	24.0	38.5	72.7	61.1	70.4	90.5	41.2	54.9	80.7	21.4	37.5	67.3

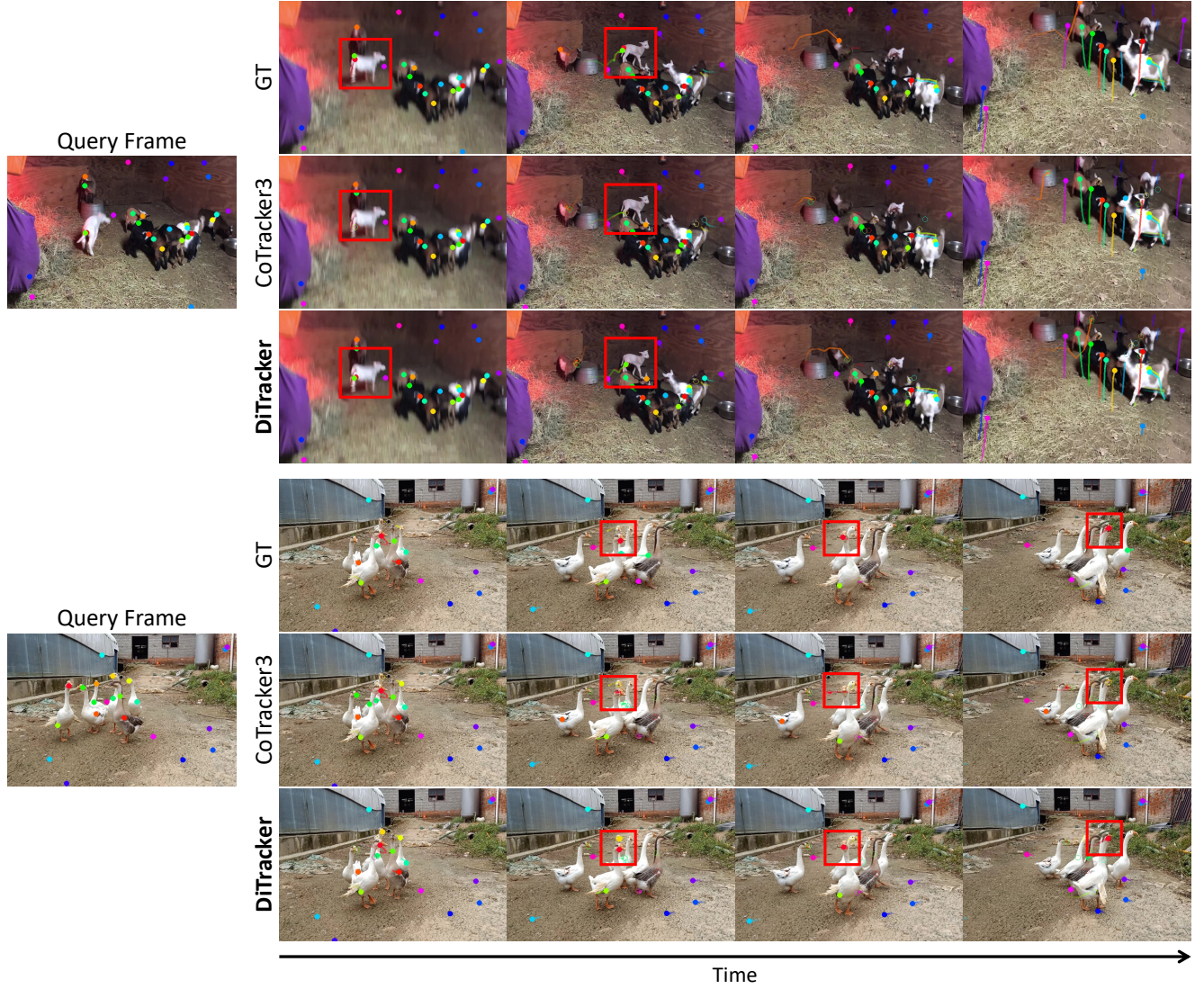


Figure 3. **Qualitative results on ITTO-MOSE [9] benchmark.** Our DiTracker predicts more accurate point trajectories under challenging real-world scenarios, including dynamic motions and occlusions, even surpassing CoTracker3 [26].

Table 5. **Quantitative evaluation on TAP-Vid-DAVIS [11] benchmark with common corruptions from ImageNet-C [21].** Our method demonstrates superior robustness consistently outperforming across most of severe corruption types including noise, blur, weather, and digital corruptions. All metrics reported as δ_{avg}^x . Best, second best and third best are highlighted.

Method	Noise			Blur				Weather				Digital			Avg.	
	Gauss.	Shot	Impulse	Defocus	Glass	Motion	Zoom	Snow	Frost	Fog	Bright	Contrast	Elastic	Pixel	JPEG	
TAPIR [12]	59.6	59.1	58.5	62.7	61.7	57.0	53.5	61.8	58.4	63.8	69.8	65.6	36.0	22.7	41.0	55.4
TAPTRv2 [34]	64.1	61.8	61.7	64.7	60.7	56.0	55.7	62.5	67.1	72.4	75.3	64.1	32.7	22.2	39.5	59.2
BootsTAPIR [13]	53.1	67.1	64.5	64.7	63.5	59.9	56.7	66.9	67.5	71.0	73.8	71.5	38.0	23.4	57.7	59.9
LocoTrack [7]	66.7	66.4	65.8	68.4	66.5	63.6	58.4	68.0	70.1	74.1	75.1	74.4	36.2	22.6	51.9	61.7
CoTracker3 [26]	54.4	51.7	51.8	66.1	60.2	57.3	55.5	62.6	64.7	73.7	73.6	71.7	22.4	23.1	42.7	55.4
CoTracker3 [†] [26]	68.5	68.0	67.6	70.7	68.5	64.3	60.2	70.8	71.6	75.8	75.3	75.5	40.0	26.2	55.7	64.7
DiTracker	73.1	73.2	71.9	71.7	66.3	64.7	61.1	72.1	73.5	76.1	77.0	73.6	42.1	23.1	56.8	65.0

Table 6. **Ablation on LoRA adaptation and ResNet fusion.**
LoRA adaptation and fusing ResNet yields best improvement.

	DiT LoRA	ResNet	DAVIS		
			AJ \uparrow	$<\delta_{\text{avg}}^x\uparrow$	OA \uparrow
(I)	\times	\times	32.2	50.0	61.6
(II)	\times	\checkmark	37.9	60.4	60.9
(III)	\checkmark	\times	46.2	63.6	76.1
(IV)	\checkmark	\checkmark	50.2	68.4	75.0

Table 7. **Ablation on matching cost fusion mechanism.** Comparing fusion strategies shows that cost-level fusion, especially concatenation, yields the best overall improvement.

	Cost Fusion	DAVIS		
		AJ \uparrow	$<\delta_{\text{avg}}^x\uparrow$	OA \uparrow
(I)	Only DiT	41.0	56.3	75.7
(II)	(I) + ResNet feature concat	41.8	56.9	74.7
(III)	(I) + ResNet cost sum	43.7	58.5	74.6
(IV)	(I) + ResNet cost concat	43.7	59.5	74.0

384 \times 512 input resolution, batch size of 1, and 5,000 training steps.

LoRA adaptation and ResNet fusion. Table 6 analyzes each component’s contribution. Comparing frozen DiT features (I) with LoRA-adapted DiT (III) shows a substantial 14.0% p improvement, demonstrating that adapting the generative feature distribution to tracking is essential despite strong pretrained correspondence capabilities. Adding ResNet fusion (IV) yields a further 4.0% p improvement to 50.2% AJ, validating complementary strengths: DiT provides robust global matching under challenging conditions, while ResNet captures fine-grained local details. Both components are critical for optimal performance.

Cost fusion strategy. Table 7 compares fusion strategies for combining DiT and ResNet features. Feature-level concatenation (II) outperforms DiT-only (I) but underperforms cost-level fusion (III, IV), indicating that direct feature concatenation disrupts DiT’s feature distribution and degrades matching capability. This validates preserving DiT’s internal matching mechanism by fusing at the cost level. For cost fusion, we compute ResNet costs using the

same softmax formulation as DiT, then compare averaging (III) versus concatenation (IV). While both achieve similar AJ, concatenation yields 1.0% p higher δ_{avg}^x by allowing the tracking head to learn adaptive weighting between cost sources—leveraging DiT’s robust matching and ResNet’s local precision—whereas averaging applies fixed uniform weights.

7. Conclusion

In this paper, we explore video DiTs as robust feature backbones for point tracking. Through systematic analysis, we demonstrate that pre-trained video DiT features exhibit strong robustness to real-world challenges including motion blur, large displacements, and occlusions. These capabilities stem from large-scale pretraining on real-world videos with full 3D attention mechanisms that capture temporally consistent features and generalizable motion priors. Building on these insights, we propose **DiTracker**, a lightweight framework that combines LoRA-based adaptation with softmax cost computation to preserve the model’s internal matching capabilities, while introducing feature fusion to integrate video DiT’s global matching strength with ResNet’s local precision. DiTracker achieves state-of-the-art performance on challenging benchmarks with significantly fewer training iterations, demonstrating the effectiveness of video DiTs as feature backbones for point tracking.

Appendix

A. Feature Backbone Comparison

Self-supervised vision foundation models. DINOv2 [45] is a self-supervised vision transformer and DINOv3 [50] extends DINOv2 by scaling both dataset and model size, producing high-quality dense features. For evaluation, we use DINOv2-B/14 and DINOv3-B/16, distilled versions from each original model, with 30×45 feature resolution.

Self-supervised video models. V-JEPA2 [1] is a masked prediction-based self-supervised model trained on large-scale video data, extending the original V-JEPA by scaling both model size and training data. The model compresses the temporal dimension by $1/2$ during patch embedding. To prevent feature smoothing from temporal compression, we repeat each frame twice to obtain one-to-one frame-mapped features, using 480×720 input resolution and extracting features from the 23rd layer, which we empirically found to provide the best matching performance.

B. Implementation Detail

B.1. Hyperparameters

Video DiT feature extraction. Following Nam et al. [44], we extract features from the 18th layer of CogVideoX-2B [61]. To select the optimal attention head, we analyze zero-shot point tracking performance across all attention heads in this layer. Figure 4 shows that the 3rd head achieves the highest accuracy. Using a single head instead

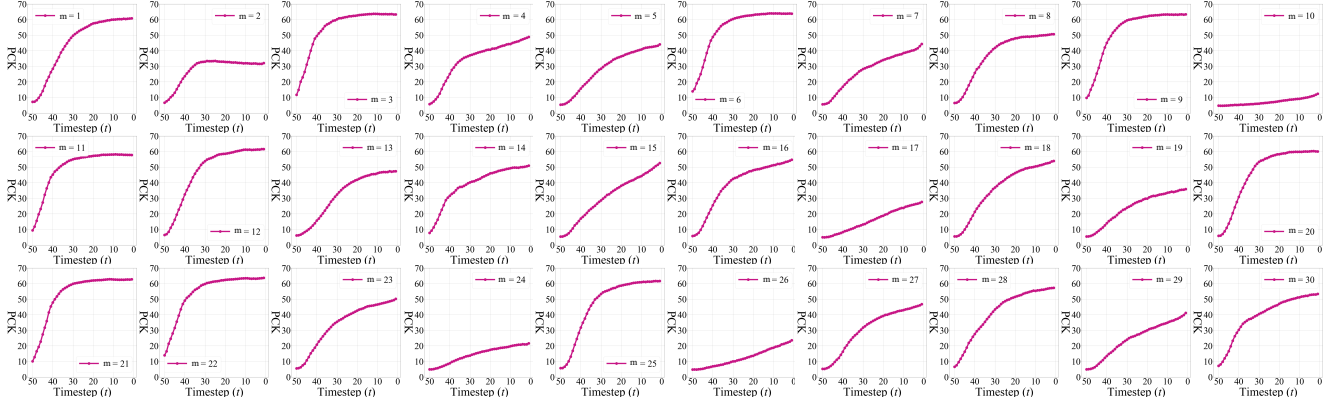


Figure 4. Attention head analysis in 17th layer of CogVideoX-2B.

Table 8. **Computation cost.** We compare inference time, throughput, and model complexity against CoTracker3 [26] using 8 frames on a single RTX A6000 GPU.

Method	Inference Time (s)						Throughput (points/sec)	FLOPs per point (G)
	10^0 point	10^1 points	10^2 points	10^3 points	10^4 points	10^5 points		
CoTracker3 [26]	0.08	0.08	0.08	0.26	2.44	OOM	4100.71	0.70
DiTracker	2.42	2.43	2.45	2.53	3.69	OOM	2707.04	1.28

of concatenating all heads significantly reduces memory requirements while maintaining strong performance.

Architecture and training. We use the following hyperparameters: feature pyramid with $S = 4$ scales, local correlation radius $\delta = 3$, model stride $r = 4$, LoRA rank 128, channel dimension $d = 64$, maximum sequence length of 46 frames, batch size of 4, and input resolution 480×720 . This resolution is chosen based on CogVideoX-2B’s strong zero-shot performance. Due to computational constraints, we use these modest hyperparameters rather than scaling to the larger batch sizes or longer sequences employed in some prior work. Nevertheless, our results demonstrate that the superior quality of video DiT features enables state-of-the-art performance even with limited training resources.

B.2. Evaluation Protocol

We adopt the evaluation metrics established by the TAP-Vid benchmark [11]. For tracking accuracy, we use δ_{avg}^x , which measures the percentage of correctly tracked visible points across multiple distance thresholds (1, 2, 4, 8, and 16 pixels), averaged to provide a single accuracy score. For visibility prediction, we report Occlusion Accuracy (OA), defined as the binary classification accuracy for determining whether each point is visible or occluded. To capture overall performance, we use Average Jaccard (AJ), which jointly evaluates both trajectory precision and visibility prediction by computing the intersection-over-union of correctly tracked visible points.

Following standard practice, we resize all videos to

256×256 resolution for evaluation on both TAP-Vid-DAVIS, TAP-Vid-Kinetics, and ITTO-MOSE benchmarks. After resizing, videos are interpolated to each model’s native input resolution for feature extraction, then predictions are mapped back to the 256×256 evaluation space for metric computation.

C. Qualitative Results

Figure 5, 6 and 7 shows visualizations on ITTO-MOSE, TAP-Vid-DAVIS, and TAP-Vid-DAVIS with corruptions from ImageNet-C [21]. Our method produces more accurate and stable trajectories across both benchmarks, demonstrating superior robustness even with substantially fewer training resources than CoTracker3 [26].

D. Limitations

While our work demonstrates the effectiveness of video DiT features for point tracking, there remain opportunities for improvement that we leave for future work. As shown in Table 8, DiTracker requires more inference time and memory compared to CoTracker3 due to the computational cost of extracting features from the large video diffusion model. This is a common trade-off when using foundation models—superior performance comes at increased computational cost.

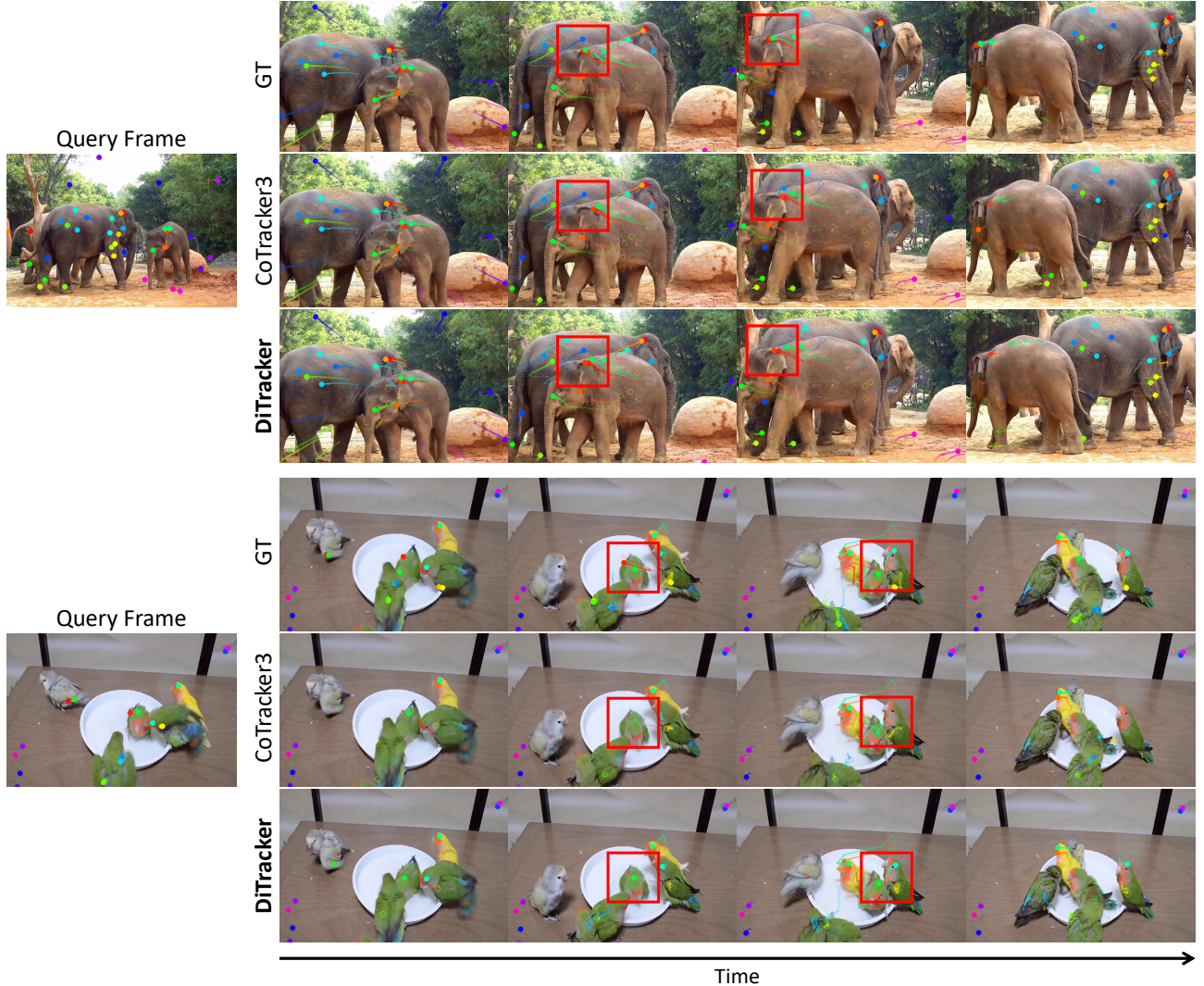


Figure 5. **Qualitative results on ITTO-MOSE [9] benchmark.** Our DiTracker predicts more smooth and accurate point trajectories under challenging real-world scenarios, including large displacement, motion blur, and occlusions, even surpassing CoTracker3 [26].

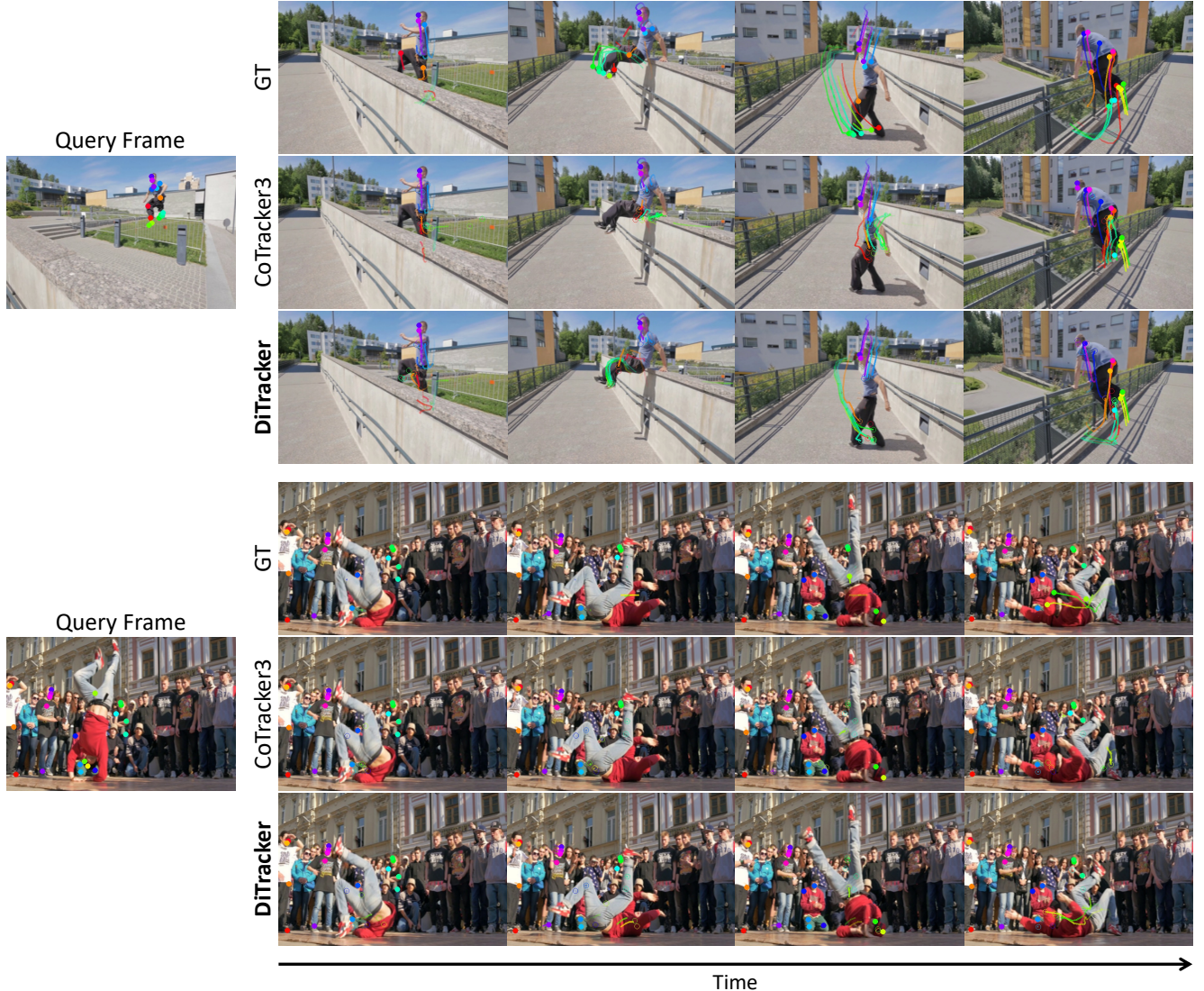


Figure 6. **Qualitative results on TAP-Vid-DAVIS [11].** Our DiTracker predicts more accurate point trajectories under large displacements between the query frame and final frame compared to CoTracker3 [26].

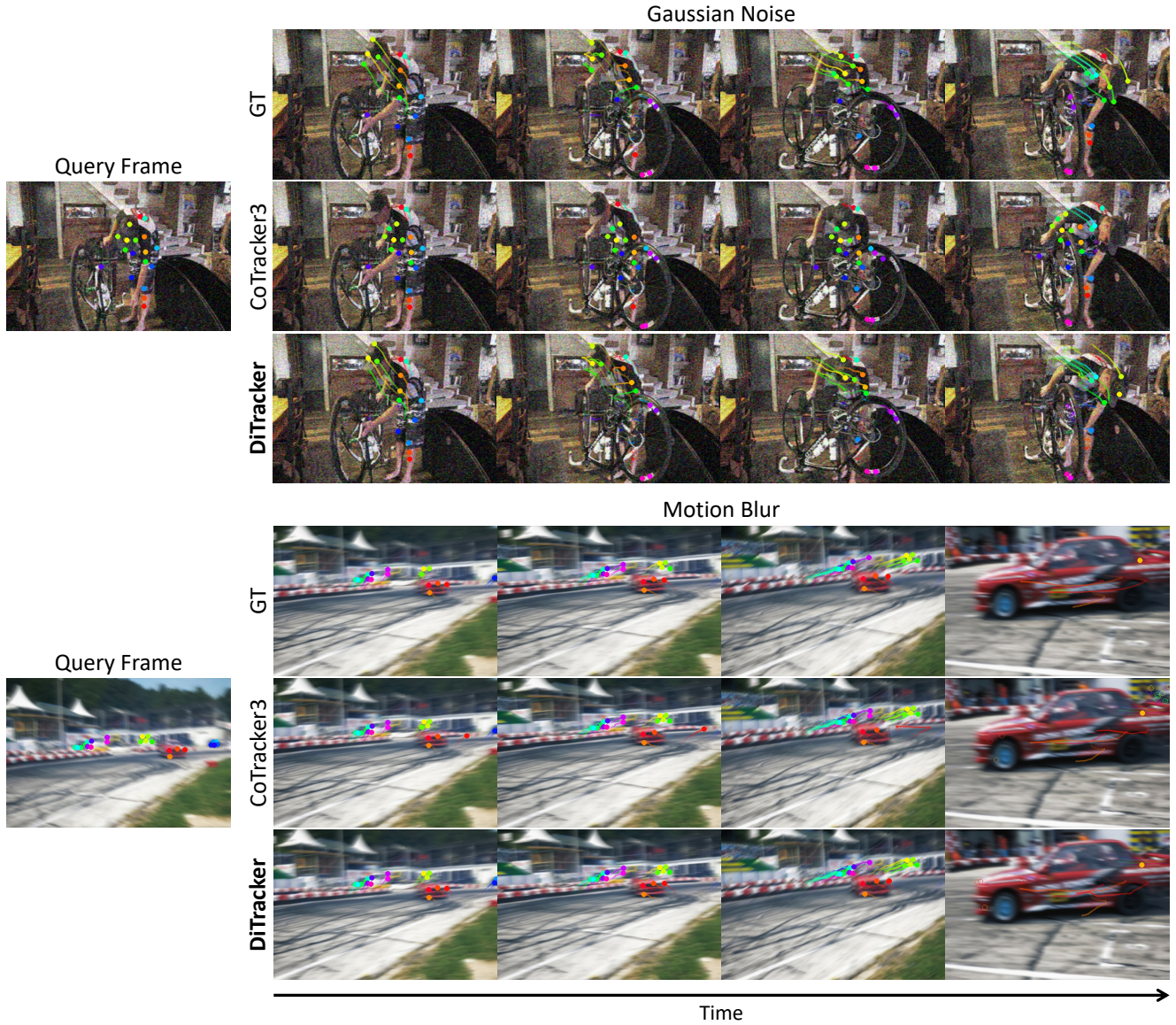


Figure 7. **Qualitative results on TAP-Vid-DAVIS [11] with corruptions from ImageNet-C [21].** Our DiTracker predicts more accurate point trajectories under gaussian noise and motion blur corruptions compared to CoTracker3 [26].

References

[1] Mido Assran, Adrien Bardes, David Fan, Quentin Garrido, Russell Howes, Matthew Muckley, Ammar Rizvi, Claire Roberts, Koustuv Sinha, Artem Zholus, et al. V-JEPA 2: Self-supervised video models enable understanding, prediction and planning. *arXiv preprint arXiv:2506.09985*, 2025. 3, 4, 10

[2] Görkay Aydemir, Weidi Xie, and Fatma Güney. Can visual foundation models achieve long-term point tracking? In *EC-CVW*, 2024. 2

[3] Görkay Aydemir, Xiongyi Cai, Weidi Xie, and Fatma Güney. Track-On: Transformer-based online point tracking with memory. In *ICLR*, 2025. 2

[4] Arjun Balasingam, Joseph Chandler, Chenning Li, Zhoutong Zhang, and Hari Balakrishnan. DriveTrack: A benchmark for long-range point tracking in real-world videos. In *CVPR*, pages 22488–22497, 2024. 2

[5] Joao Carreira and Andrew Zisserman. Quo vadis, action recognition? a new model and the kinetics dataset. In *CVPR*, pages 6299–6308, 2017. 6

[6] Seokju Cho, Jiahui Huang, Seungryong Kim, and Joon-Young Lee. FlowTrack: Revisiting optical flow for long-range dense tracking. In *CVPR*, pages 19268–19277, 2024. 2

[7] Seokju Cho, Jiahui Huang, Jisu Nam, Honggyu An, Seungryong Kim, and Joon-Young Lee. Local all-pair correspondence for point tracking. In *ECCV*, pages 306–325, 2024. 1, 2, 7, 8, 9

[8] Seokju Cho, Jiahui Huang, Seungryong Kim, and Joon-Young Lee. Seurat: From moving points to depth. In *CVPR*, pages 7211–7221, 2025. 1, 2

[9] Ilona Demler, Saumya Chauhan, and Georgia Gkioxari. Is this tracker on? a benchmark protocol for dynamic tracking. *NeurIPS*, 2025. 2, 4, 6, 7, 8, 12

[10] Henghui Ding, Chang Liu, Shuting He, Xudong Jiang, Philip HS Torr, and Song Bai. MOSE: A new dataset for video object segmentation in complex scenes. In *ICCV*, pages 20224–20234, 2023. 7

[11] Carl Doersch, Ankush Gupta, Larisa Markeeva, Adria Recasens, Lucas Smaira, Yusuf Aytar, Joao Carreira, Andrew Zisserman, and Yi Yang. TAP-Vid: A benchmark for tracking any point in a video. *NeurIPS*, 35:13610–13626, 2022. 1, 2, 3, 4, 6, 7, 9, 10, 13, 14

[12] Carl Doersch, Yi Yang, Mel Vecerik, Dilara Gokay, Ankush Gupta, Yusuf Aytar, Joao Carreira, and Andrew Zisserman. TAPIR: Tracking any point with per-frame initialization and temporal refinement. In *ICCV*, pages 10061–10072, 2023. 1, 2, 7, 8, 9

[13] Carl Doersch, Pauline Luc, Yi Yang, Dilara Gokay, Skanda Koppula, Ankush Gupta, Joseph Heyward, Ignacio Rocco, Ross Goroshin, Joao Carreira, et al. BootsTAP: Bootstrapped training for tracking-any-point. In *ACCV*, pages 3257–3274, 2024. 2, 7, 8, 9

[14] Chaofan Gan, Yuanpeng Tu, Xi Chen, Tieyuan Chen, Yuxi Li, Mehrtash Harandi, and Weiyao Lin. Unleashing diffusion transformers for visual correspondence by modulating massive activations. *NeurIPS*, 2025. 2, 3

[15] Daniel Geng, Charles Herrmann, Junhwa Hur, Forrester Cole, Serena Zhang, Tobias Pfaff, Tatiana Lopez-Guevara, Carl Doersch, Yusuf Aytar, Michael Rubinstein, Chen Sun, Oliver Wang, Andrew Owens, and Deqing Sun. Motion prompting: Controlling video generation with motion trajectories. In *CVPR*, 2025. 1

[16] Kristen Grauman, Andrew Westbury, Eugene Byrne, Zachary Chavis, Antonino Furnari, Rohit Girdhar, Jackson Hamburger, Hao Jiang, Miao Liu, Xingyu Liu, et al. Ego4D: Around the world in 3,000 hours of egocentric video. In *CVPR*, pages 18995–19012, 2022. 7

[17] Klaus Greff, Francois Belletti, Lucas Beyer, Carl Doersch, Yilun Du, Daniel Duckworth, David J. Fleet, Dan Gnanapragasam, Florian Golemo, Charles Herrmann, et al. Kubric: A scalable dataset generator. In *CVPR*, pages 3749–3761, 2022. 1, 2, 6

[18] Adam W. Harley, Zhaoyuan Fang, and Katerina Fragkiadaki. Particle video revisited: Tracking through occlusions using point trajectories. In *ECCV*, pages 59–75. Springer, 2022. 2

[19] Adam W. Harley, Yang You, Xinglong Sun, Yang Zheng, Nikhil Raghuraman, Yunqi Gu, Sheldon Liang, Wen-Hsuan Chu, Achal Dave, Pavel Tokmakov, et al. AllTracker: Efficient dense point tracking at high resolution. In *ICCV*, 2025. 1

[20] Kaiming He, Xiangyu Zhang, Shaoqing Ren, and Jian Sun. Deep residual learning for image recognition. In *CVPR*, pages 770–778, 2016. 1, 2, 3

[21] Dan Hendrycks and Thomas Dietterich. Benchmarking neural network robustness to common corruptions and perturbations. In *ICLR*, 2019. 2, 4, 7, 9, 11, 14

[22] Jonathan Ho, Ajay Jain, and Pieter Abbeel. Denoising diffusion probabilistic models. *NeurIPS*, 33:6840–6851, 2020. 3

[23] Lingyi Hong, Wenchao Chen, Zhongying Liu, Wei Zhang, Pinxue Guo, Zhaoyu Chen, and Wenqiang Zhang. LVOS: A benchmark for long-term video object segmentation. In *ICCV*, pages 13480–13492, 2023. 7

[24] Edward J. Hu, Yelong Shen, Phillip Wallis, Zeyuan Allen-Zhu, Yuanzhi Li, Shean Wang, Lu Wang, Weizhu Chen, et al. LoRA: Low-rank adaptation of large language models. *ICLR*, 1(2):3, 2022. 2, 5

[25] Linyi Jin, Richard Tucker, Zhengqi Li, David Fouhey, Noah Snavely, and Aleksander Holynski. Stereo4D: Learning how things move in 3D from internet stereo videos. In *CVPR*, pages 10497–10509, 2025. 2

[26] Nikita Karaev, Iurii Makarov, Jianyuan Wang, Natalia Neverova, Andrea Vedaldi, and Christian Rupprecht. Co-Tracker3: Simpler and better point tracking by pseudo-labelling real videos. *arXiv preprint arXiv:2410.11831*, 2024. 1, 2, 3, 4, 6, 7, 8, 9, 10, 11, 12, 13, 14

[27] Nikita Karaev, Ignacio Rocco, Benjamin Graham, Natalia Neverova, Andrea Vedaldi, and Christian Rupprecht. Co-Tracker: It is better to track together. In *ECCV*, pages 18–35, 2024. 2

[28] Bingxin Ke, Anton Obukhov, Shengyu Huang, Nando Metzger, Rodrigo Caye Daudt, and Konrad Schindler. Repurposing diffusion-based image generators for monocular depth estimation. In *CVPR*, pages 9492–9502, 2024. 2, 3

[29] Inès Hyeonsu Kim, Seokju Cho, Jiahui Huang, Jung Yi, Joon-Young Lee, and Seungryong Kim. Exploring temporally-aware features for point tracking. In *CVPR*, pages 1962–1972, 2025. 1, 2

[30] Inès Hyeonsu Kim, Seokju Cho, Jiahyeok Koo, Junghyun Park, Jiahui Huang, Joon-Young Lee, and Seungryong Kim. Learning to track any points from human motion. *arXiv preprint arXiv:2507.06233*, 2025. 2

[31] Weijie Kong, Qi Tian, Zijian Zhang, Rox Min, Zuozhuo Dai, Jin Zhou, Jiangfeng Xiong, Xin Li, Bo Wu, Jianwei Zhang, et al. HunyuanVideo: A systematic framework for large video generative models. *arXiv preprint arXiv:2412.03603*, 2024. 3, 4

[32] Guillaume Le Moing, Jean Ponce, and Cordelia Schmid. Dense optical tracking: Connecting the dots. In *CVPR*, pages 19187–19197, 2024. 2

[33] Hongyang Li, Hao Zhang, Shilong Liu, Zhaoyang Zeng, Feng Li, Bohan Li, Tianhe Ren, and Lei Zhang. TAPTRv2: Attention-based position update improves tracking any point. *NeurIPS*, 37:101074–101095, 2024. 2

[34] Hongyang Li, Hao Zhang, Shilong Liu, Zhaoyang Zeng, Tianhe Ren, Feng Li, and Lei Zhang. TAPTR: Tracking any point with transformers as detection. In *ECCV*, pages 57–75. Springer, 2024. 2, 7, 8, 9

[35] Xinghui Li, Jingyi Lu, Kai Han, and Victor Adrian Prisacariu. SD4Match: Learning to prompt stable diffusion model for semantic matching. In *CVPR*, pages 27558–27568, 2024. 3

[36] Zhimin Li, Jianwei Zhang, Qin Lin, Jiangfeng Xiong, Yanxin Long, Xinch Deng, Yingfang Zhang, Xingchao Liu, Minbin Huang, Zedong Xiao, et al. Hunyuan-DIT: A powerful multi-resolution diffusion transformer with fine-grained chinese understanding. *arXiv preprint arXiv:2405.08748*, 2024. 1, 2, 4

[37] Ji Lin, Chuang Gan, and Song Han. TSM: Temporal shift module for efficient video understanding. In *ICCV*, pages 7083–7093, 2019. 2

[38] Yaron Lipman, Ricky TQ Chen, Heli Ben-Hamu, Maximilian Nickel, and Matt Le. Flow matching for generative modeling. *arXiv preprint arXiv:2210.02747*, 2022. 3

[39] Yuhan Liu, Jingwen Fu, Yang Wu, Kangyi Wu, Pengna Li, Jiayi Wu, Sanping Zhou, and Jingmin Xin. Mind the gap: Aligning vision foundation models to image feature matching. *arXiv preprint arXiv:2507.10318*, 2025. 3

[40] Grace Luo, Lisa Dunlap, Dong Huk Park, Aleksander Holynski, and Trevor Darrell. Diffusion hyperfeatures: Searching through time and space for semantic correspondence. *NeurIPS*, 36:47500–47510, 2023. 3

[41] Benyuan Meng, Qianqian Xu, Zitai Wang, Xiaochun Cao, and Qingming Huang. Not all diffusion model activations have been evaluated as discriminative features. *NeurIPS*, 37: 55141–55177, 2024. 2, 3

[42] Jisu Nam, Heesu Kim, DongJae Lee, Siyoon Jin, Seungryong Kim, and Seunggyu Chang. DreamMatcher: Appearance matching self-attention for semantically-consistent text-to-image personalization. In *CVPR*, pages 8100–8110, 2024. 3

[43] Jisu Nam, Gyuseong Lee, Sunwoo Kim, Hyeonsu Kim, Hyeoungwon Cho, Seyeon Kim, and Seungryong Kim. Diffusion model for dense matching. In *ICLR*, 2024. 2, 3, 7

[44] Jisu Nam, Soowon Son, Dahyun Chung, Jiyoung Kim, Siyoon Jin, Junhwa Hur, and Seungryong Kim. Emergent temporal correspondences from video diffusion transformers. *NeurIPS*, 2025. 2, 3, 10

[45] Maxime Oquab, Timothée Darcet, Théo Moutakanni, Huy Vo, Marc Szafraniec, Vasil Khalidov, Pierre Fernandez, Daniel Haziza, Francisco Massa, Alaaeldin El-Nouby, et al. DINOv2: Learning robust visual features without supervision. *arXiv preprint arXiv:2304.07193*, 2023. 2, 3, 4, 10

[46] Jordi Pont-Tuset, Federico Perazzi, Sergi Caelles, Pablo Arbeláez, Alex Sorkine-Hornung, and Luc Van Gool. The 2017 davis challenge on video object segmentation. *arXiv preprint arXiv:1704.00675*, 2017. 6

[47] Jinyuan Qu, Hongyang Li, Shilong Liu, Tianhe Ren, Zhaoyang Zeng, and Lei Zhang. TAPTRv3: Spatial and temporal context foster robust tracking of any point in long video. *arXiv preprint arXiv:2411.18671*, 2024. 2

[48] Robin Rombach, Andreas Blattmann, Dominik Lorenz, Patrick Esser, and Björn Ommer. High-resolution image synthesis with latent diffusion models. In *CVPR*, pages 10684–10695, 2022. 2, 3

[49] Peter Sand and Seth Teller. Particle video: Long-range motion estimation using point trajectories. *IJCV*, 80(1):72–91, 2008. 2

[50] Oriane Siméoni, Huy V Vo, Maximilian Seitzer, Federico Baldassarre, Maxime Oquab, Cijo Jose, Vasil Khalidov, Marc Szafraniec, Seungeun Yi, Michaël Ramamonjisoa, et al. DINOv3. *arXiv preprint arXiv:2508.10104*, 2025. 3, 4, 10

[51] Nick Stracke, Stefan Andreas Baumann, Kolja Bauer, Frank Fundel, and Björn Ommer. CleanDIFT: Diffusion features without noise. In *CVPR*, pages 117–127, 2025. 3

[52] Luming Tang, Menglin Jia, Qianqian Wang, Cheng Perng Phoo, and Bharath Hariharan. Emergent correspondence from image diffusion. *NeurIPS*, 36:1363–1389, 2023. 2, 3

[53] Narek Tumanyan, Assaf Singer, Shai Bagon, and Tali Dekel. DINO-Tracker: Taming DINO for self-supervised point tracking in a single video. In *ECCV*, pages 367–385, 2024. 2

[54] Mel Vecerik, Carl Doersch, Yi Yang, Todor Davchev, Yusuf Aytar, Guangyao Zhou, Raia Hadsell, Lourdes Agapito, and Jon Scholz. RoboTAP: Tracking arbitrary points for few-shot visual imitation. In *ICRA*, pages 5397–5403, 2024. 1

[55] Team Wan, Ang Wang, Baole Ai, Bin Wen, Chaojie Mao, Chen-Wei Xie, Di Chen, Feiwu Yu, Haiming Zhao, Jianxiao Yang, et al. Wan: Open and advanced large-scale video generative models. *arXiv preprint arXiv:2503.20314*, 2025. 1, 2, 3, 4

[56] Qianqian Wang, Yen-Yu Chang, Ruojin Cai, Zhengqi Li, Bharath Hariharan, Aleksander Holynski, and Noah Snavely. Tracking everything everywhere all at once. In *ICCV*, pages 19795–19806, 2023. 2

- [57] Qianqian Wang, Vickie Ye, Hang Gao, Jake Austin, Zhengqi Li, and Angjoo Kanazawa. Shape of motion: 4D reconstruction from a single video. In *ICCV*, 2025. [1](#)
- [58] Yuxi Xiao, Qianqian Wang, Shangzhan Zhang, Nan Xue, Sida Peng, Yujun Shen, and Xiaowei Zhou. SpatialTracker: Tracking any 2D pixels in 3D space. In *CVPR*, pages 20406–20417, 2024. [1](#), [2](#)
- [59] Jiarui Xu, Sifei Liu, Arash Vahdat, Wonmin Byeon, Xiaolong Wang, and Shalini De Mello. Open-vocabulary panoptic segmentation with text-to-image diffusion models. In *CVPR*, pages 2955–2966, 2023. [2](#), [3](#)
- [60] Fei Xue, Sven Elflein, Laura Leal-Taixé, and Qunjie Zhou. MATCHA: Towards matching anything. In *CVPR*, pages 27081–27091, 2025. [3](#)
- [61] Zhuoyi Yang, Jiayan Teng, Wendi Zheng, Ming Ding, Shiyu Huang, Jiazheng Xu, Yuanming Yang, Wenyi Hong, Xiaohan Zhang, Guanyu Feng, et al. CogVideoX: Text-to-video diffusion models with an expert transformer. *arXiv preprint arXiv:2408.06072*, 2024. [1](#), [2](#), [3](#), [4](#), [10](#)
- [62] Junyi Zhang, Charles Herrmann, Junhwa Hur, Luisa Polania Cabrera, Varun Jampani, Deqing Sun, and Ming-Hsuan Yang. A tale of two features: Stable diffusion complements dino for zero-shot semantic correspondence. *NeurIPS*, 36: 45533–45547, 2023. [2](#), [3](#)
- [63] Junyi Zhang, Charles Herrmann, Junhwa Hur, Eric Chen, Varun Jampani, Deqing Sun, and Ming-Hsuan Yang. Telling left from right: Identifying geometry-aware semantic correspondence. In *CVPR*, pages 3076–3085, 2024. [3](#)
- [64] Artem Zholus, Carl Doersch, Yi Yang, Skanda Koppula, Viorica Patraucean, Xu Owen He, Ignacio Rocco, Mehdi SM Sajjadi, Sarath Chandar, and Ross Goroshin. TAPNext: Tracking any point (TAP) as next token prediction. In *ICCV*, 2025. [1](#)